Multiscale Flotation Testing for the Recovery of REEs-Bearing Fluorapatite from a Finnish Carbonatite Complex Deposit Using Conventional Collectors and Lignin Nanoparticles

Panagiotis Michail Angelopoulos * , Xiao Sheng Yang , Georgios Anastassakis , Nikolaos Koukoulis , Paul Christakopoulos , Maria Taxiarchou

Posted Date: 23 April 2025

doi: 10.20944/preprints202504.1931.v1

Keywords: froth flotation; apatite; Rare Earth Elements (REE); organosolv lignin

 doi:10.20944/preprints202504.1931.v1

Article

Multiscale Flotation Testing for the Recovery of REEs-Bearing Fluorapatite from a Finnish Carbonatite Complex Deposit Using Conventional Collectors and Lignin Nanoparticles

Panagiotis M. Angelopoulos [1,*], Xiao Sheng Yang [2], Georgios Anastassakis [3], Nikolaos Koukoulis [3], Paul Christakopoulos [4] and Maria Taxiarchou [1]

[1] Laboratory of Metallurgy, School of Mining and Metallurgical Engineering, National Technical University of Athens, Iroon Polytechniou 9 str., GR 15780 Zografou Campus, Athens, Greece
[2] Mintec Laboratory, Geological Survey of Finland (GTK), Vuorimiehentie 5, P.O. Box 96, FI-02151 Espoo, Finland
[3] Laboratory of Mineral Processing, School of Mining and Metallurgical Engineering, National Technical University of Athens, Iroon Polytechniou 9 str., GR 15780 Zografou Campus, Athens, Greece
[4] Division of Chemical Engineering, Department of Civil, Environmental and Natural Resources Engineering, Luleå University of Technology, Porsön Luleå, Sweden
* Correspondence: pangelopoulos@metal.ntua.gr

Abstract: Apatite and rare earth elements (REEs) are vital to the European Union's economic growth and resource security, given their essential roles in fertilizers, green technologies, and high-tech applications. To meet rising demand and reduce reliance on imports, the exploitation of domestic deposits has become increasingly important. This study investigates the beneficiation potential of ore from a carbonatite complex (Finland), focusing on the recovery of fluorapatite concentrate through froth flotation. The research addresses two key objectives: evaluating the potential for REE enrichment alongside fluorapatite concentration using conventional anionic and amine-based reagents, and assessing separation efficiency when partially substituting the most effective conventional collectors with bio-based organosolv lignin nanoparticles. Adequate recovery rates for apatite and REEs were achieved using common anionic collectors, such as hydroxamate and sarcosine, yielding P grades of 23.4% and 21.5%, and recoveries of 96.4% and 89.2%, respectively. Importantly, concentrate quality remained stable with up to 30% reduction of conventional collectors and addition of organosolv lignin. Bench-scale trials further validated the approach, demonstrating that lanthanum and cerium recoveries exceeded 71%, alongside satisfactory apatite recovery. The findings highlight lignin nanoparticles as an environmentally friendly alternative to conventional reagents in apatite flotation, offering potential to reduce the environmental footprint of the process without compromising flotation kinetics or concentrate quality.

Keywords: froth flotation; apatite; Rare Earth Elements (REE); organosolv lignin

1. Introduction

Rare Earth Elements (REEs) are considered valuable minerals that have a variety of applications in different industries such as tech, automotive, industrial etch [1]. They consist of the 15 lanthanide series elements (La, Pr, Ce, Eu, Pm, Ho, Nd, Gd, Yb, Dy, Sm, Er, Tm, Tb, and Lu) with the addition of Sc and Y [2]. With an increasing demand of REEs for clean energy market and advanced materials, alternative sources for minerals should be implemented. As of 2023, China with an annual production of around 240000 metric tons holds of 68.57 % of the annual production share of REEs followed by US at 12.29%, and Myanmar at 20.86 %, while Europe does not produce yet, despite the fact that REEs were recognized by the European Commission in 2017 as one of the vital raw materials (CRMs) to

 doi:10.20944/preprints202504.1931.v1

the European economy [3,4]. There are however, few identified REE deposits in the Europe with those associated with Mesoproterozoic rift-related magmatism in Greenland and Sweden, and with Neoproterozoic to Palaeozoic carbonatites across Greenland and the Fennoscandian Shield being the most important ones, but none of them are currently under exploitation [5,6].

Apatite, a group of phosphate minerals, can incorporate substantial amounts of REEs into their crystalline structure, and has been identified as an important host for rare earth and secondary source of them. [7–10]. This is due to enrichment of REE within apatite, that can be done by two processes; the first is the substitution of REE^{3+} and Na^{+} for Ca^{2+} within the apatite, while the second is P^{5+} substituted with REE^{3+} and Si^{4+} with the end member of the second substitution being britholite, a mineral heavily enriched in REE [11,12]. As a consequence, the REE content can go as high as 0.1 to 3.5 %, as shown by Owens et al. on a list presenting REE-hosting apatite deposits [8].

The carbonatite complex, located in North Savo, Finland is a typical case of REE-enriched apatite deposit. The complex comprises of intermixed carbonatite and glimmerite, with almost all rocks constituting phosphate ore with apatite content of about ≈10 % [13,14]. The mine production was 11 Mt/y, and ore reserves were estimated to 234 Mt at an average grade of 4 wt. %, and has been identified as potential source of REE and F [13,14]. REE content in apatite was estimated to 0.3-0.4 wt. % ,while the fluorine content for the apatite ranges from 2.3 to 3.5 % [15,16].

Further to the primary sources of REEs, the wide range of uses and the rising global demand have led to exploration of alternative sources beyond regular mining, with the recovery from industrial wastes and byproducts like acid mine drainage and mine tailings being considered viable secondary sources of REEs [17,18].

Being identified as an important source of REEs, various beneficiation studies deal with the production of a valuable concentrate from ore deposits or mining tailings [19]. For the production of bastnäsite ($Ce,La(FCO_3)$), monazite ($Ce,La(PO_4)$), and xenotime (YPO_4) concentrates, which are the REE bearing minerals that have been extracted on a commercial scale, gravity, magnetic, electrostatic and flotation separation are commonly applied, with the latter being the most significant one worldwide [19–21]. The most commonly used collectors for REE minerals flotation are either hydroxamic or fatty acids [20]. Initially, fatty (carboxylic) acid was the preferred collector for bastnasite flotation due to the wide availability and low price, however considerable amounts of depressants are needed to achieve high grade and recovery in the concentrate [22]. Regarding monazite and xenotime which are found typically together in heavy metal sand deposits, the collectors that are used are similar to bastnasite (fatty acid and hydroxamate collectors) , due to similarities at surface they share [19]. On the other hand, apatite flotation is commonly done using either fatty acids like oleic acid [23,24]and sodium oleate [25], and anionic surfactants like alkyl sulfate[26], alkyl sulfonate [27]and alkyl hydroxamates[28].

Lignin is a polymer structuring the cell walls of plants, exhibiting complex structure with various functional groups, including phenolic hydroxyl, aliphatic hydroxyls and carboxyl acids, while when extracted using organic solvents (organosolv), results in a less chemically modified and more uniform product compared to other lignin types[29]. Recent studies have shown that organosolv lignin nanoparticles can be beneficial to the flotation by interacting with mineral surfaces, probably through the many functional groups [30]. Other studies have shown that lignin is beneficial to the flotation because it enhances the separation efficiency through depressing calcite [31] in scheelite-calcite system, and molybdenite in molybdenite-chalcopyrite system [32]. The use of lignin in the flotation process is of particular interest because of the environmental benefits that arise from the fact that it is biodegradable, natural and renewable biopolymer of low toxicity, as well as its abundance and cost-efficiency.

Potential use of organosolv lignin micro- and nanoparticles have been investigated by Hruzova et al. in a Cu-Ni sulfide ore (Maurliden, Sweden) and a complex Cu-Pb-Zn ore (Kristineberg, Sweden), leading to improvement to the Zn grade and recovery, Ni grade and Pb recovery [33]. In another study dealing with Kupfershiefer copper ore (Poland), it was shown that lignin nanoparticles can replace maltodextrin in final concentrate selective flotation, where it would provide the selective

 doi:10.20944/preprints202504.1931.v1

separation of copper and total organic carbon [34]. Angelopoulos et al. use organosolv lignin nanoparticles to partially replace sodium isopropyl xanthate (SIPX) in the flotation of sphalerite and pyrite/arsenopyrite from mixed sulfide ore, achieving higher sphalerite grade and higher pyrite arsenopyrite grade and recovery by 50% replacement of SIPX by lignin[35]. Recently, Bazar et al investigated the flotation of iron oxide apatite ore tailings using a combination of tall oil fatty acid-based collector (TOFA) and organosolv lignin nanoparticles focusing on the identification of synergy[36]. The study highlights a synergistic effect between OLP and the TOFA collector, suggesting that lignin might interact with TOFA, either by enhancing its adsorption onto apatite or by surface modification, leading to higher P_2O_5 grade and recovery.

The article presents an investigation on the beneficiation potential of ore originated from Finnish carbonatite complex, targeting the recovery of fluorapatite concentrate through froth flotation tests with dual aim; the identification of the possibility to achieve enrichment of REEs in parallel to the concentration of fluorapatite by evaluating the performance of different conventional reagents on that, but also the determination of the separation performance under the reduction of best-performance collectors and the addition of lignin, on application levels extending from lab- to bench scale.

2. Materials and Methods

2.1. Ore Characterization

Ore originates carbonatite ore deposits, located in central Finland. It is an open pit deposit rich in fluorapatite, calcite and phlogopite but also in REE, which is attributed to the re-equilibration of early apatite (via sub-solidus diffusion at the magmatic stage) with a fresh carbonatitic magma enriched in REEs [14]. The chemical composition of the feed and flotation products was analysed on an X-ray fluorescence The sample was homogenized and dried overnight at 105 °C, and subsequently subjected to chemical analysis on an Energy-Dispersive X-Ray Fluorescence instrument Xepos (SPECTRO A.I. GmbH). For REE analysis determination, sodium peroxide plus sodium hydroxide digestion was used and measurement was done with ICP-MS technique. Quantitative mineralogical studies were carried out by using a mineral liberation analyzer (MLA) and an electron probe micro analyzer (EPMA). The MLA equipment consists of the standard modern SEM (FEI Quanta 600) with the energy dispersive X-ray analyzer (EDAX Genesis with two detectors). The XMOD-STD and XBSE methods were used for analyzing the modal mineralogy and the mineral liberation, respectively. The EPMA was used for determining the chemical compositions of apatite in the sample.

As for the SEM images, thin polished cut of raw material was prepared by impregnating approx. 1 gr of dry matter with epoxy resin in a cylindric mold, and subsequent cutting and surface smoothing for morphological observation on a SEM (JEOL JSM-IT500LV) under accelerating voltage 20 kV, probe current 1.5nA and 12 mm working distance. Local elements identification was done by energy dispersive sensor type Ultim Max 100 (Oxford Instruments, UK).

2.2. Lignin Production and Properties

The lignin used for preparation of lignin nanoparticles was extracted by organosolv pretreatment of spruce wood chips [37]. The spruce woodchips were pretreated in 60% v/v ethanol in water solution at 183°C for 1 h. The extracted lignin was dried and dissolved in 75% v/v ethanol/water solution. Subsequently, the 5% w/v lignin in the ethanol/water solution was homogenized at 750 bar by using a pressure homogenizer (APV-2000, SPX FLOW, Charlotte, NC, USA). The homogenized liquid was further diluted by deionized water, which lead to the formation of nanoparticles. To obtain nanoparticles as a dry powder, the sample was freeze dried. The preparation process yielded nanoparticles that were smaller than 500 nm [38].

The morphology of the lignin nanoparticles was observed by scanning electron microscopy (SEM, FEI Magellan 400 field emission XHR-SEM). The samples were placed on conductive carbon tapes prior to the analysis and the images were taken at a low accelerating voltage of 3 kV and a beam

 doi:10.20944/preprints202504.1931.v1

current of 6.3 pA. For the purpose of the flotation trails the dry powder of nanoparticles was dispersed in deionized water at the concentration of 1% w/v and sonicated by ultrasound for 5 min. Subsequently, the sample was mixed before use to prevent sedimentation and increase homogeneity of the dispersion in the flotation trials. Macroscopic and microscopic view of produced lignin nanoparticles are depicted in Figure 1a and b, respectively.

Figure 1. Macroscopic (a) and microscopic view (b) of lignin nanoparticles.

2.3. Flotation Tests

The research approach that is followed in the study consists of 3 consecutive steps, depicted in Figure 2; after characterization of raw material and size control, flotation experiments were executed in lab-scale using conventional reagents, aiming to identify their efficiency in the concentration of both apatite and REEs of interest, namely cerium, lanthanum and yttrium. After evaluation of the results, two flotation experiments with best performance reagents were carried out again, applying partial substitution with OLN under different degree. Finally, process upscaling was carried out in a 13L flotation cell, where flotation scenarios of sole conventional and mixed collector with lignin were run and their performance was compared and discussed. This experimental design is favourable as it allows a systematic, stepwise evaluation of flotation reagents, starting with lab-scale tests to establish baseline performance of conventional reagents, while partial replacement of top-performing reagents with green alternatives is focused on balancing efficacy and sustainability. This progressive design minimizes risk, reduces material usage in initial trials, and ensures resource efficiency as the process moves toward full-scale application.

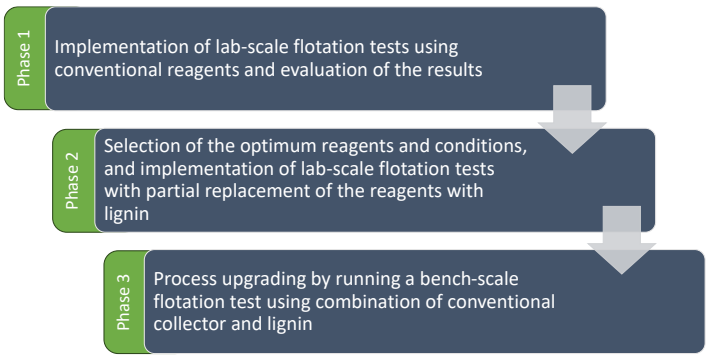

Figure 2. Research methodology.

As for the collectors used in the flotation trials, their trade name, formula and structure are presented in Table 1, and the applied flotation conditions on each trial are tabulated in Table 2. Their

 doi:10.20944/preprints202504.1931.v1

selection is based on data found in bibliography regarding the flotation of REE- hosting apatite [8,20,28,39,40].

Table 1. Tradename, formula and structure of the conventional collectors used [41].

Trade Name and Formula	Molecular Structure of the Functional Group
Aero 6494©, anionic, alkyl hydroxamate-based collector	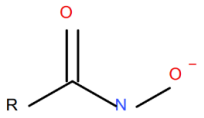
Sodium Oleate (NaOL), anionic, sodium salt of oleic acid	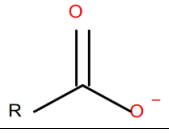
Berol A3©, sarcosine, a carboxylic acid coupled to a methylated nitrogen	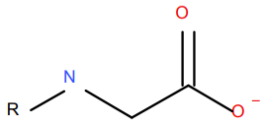

The flotation experiments were carried out under alkaline pH range between 10 and 11. Collector dosage was between 150 and 300 g/t and in most trials Na_2SiO_3 was used as depressant of phlogopite. Nanosized lignin partially replaced conventional reagents in tests 8-12 without affecting other flotation conditions.

Table 2. Lab-scale flotation tests' reagents and conditions.

Number	Reagents (g/t)						pH	Time (m)		Cell Size (L)	Pulp Density (g/L)
	Hydroxamate (Aero 6494®)	Ling-chain fatty acid (NaOL)	Sacrosine (Berol A3®)	Organosolv Nanosized lignin	Replacement **	Na_2SiO_3		Conditioning	Flotation		
1*	250					800	10	5	9	2.5	300
2	250					800	10	5	9	2.5	300
3		300					10.5	5	6	2.5	300
4		350				1400	10.5	5	9	2.5	300
5			300				11	5	9	2.5	300
6	150					800	10	5	12	2.5	300
7	300					800	10	5	9	2.5	300
8			240	60	20		11	5	9	2.5	300
9			210	90	30		11	5	9	2.5	300
10	210			90	30	800	10	5	9	2.5	300
11			180	120	40		11	5	9	2.5	300
12	200			200	50	800	10	5	9	2.5	300

*Heated at 55 °C. ** % replacement of conventional reagent.

The steps of the conditioning and flotation procedure are depicted in Figure 3.

 doi:10.20944/preprints202504.1931.v1

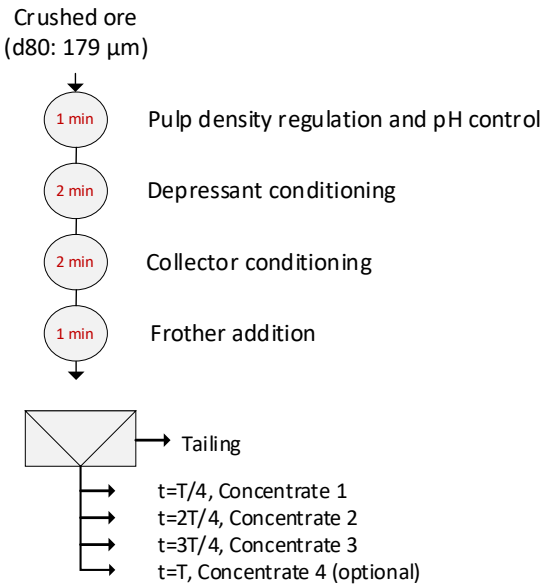

Figure 3. Sequence of steps in conditioning and flotation.

The interaction of minerals with reagents was investigated through Fourier-transform infrared spectroscopy (FTIR) with the transmission KBr pellet technique on a PerkinElmer Spectrum 100 FT-IR device. Hydrophobicity/hydrophilicity of pure minerals was evaluated using a Rame Hart contact angle goniometer Model 210. Pure fluorapatite and phlogopite crystals were subjected to fine polishing using Al abrasive paper to create flat surfaces. Subsequently, the minerals were treated with different reagents, and contact angle of distilled water droplet was measured fivefold with the goniometer.

3. Results and Discussion

3.1. Feed Properties

The chemical composition of the sample is presented in Table 3, while mineralogical one in Table 4 as follows from the mineral liberation analysis. The sample consists of phlogopite in content exceeding 55 %, followed by calcite and apatite by approx. 16.6 and 8.9 %, respectively. The chemical analysis, which is in line with the mineralogical one, revealed the high content of the sample in silicon and magnesium, which is major component of phlogopite, calcium for calcite and phosphorous for apatite. Such findings are confirmed by the micrographs presented in Figure 5, and the depicted local chemical analyses that allowed identification of main mineralogical phases of the sample, namely phlogopite, apatite, magnetite, calcite and biotite.

Table 3. Chemical analysis of the feed.

Oxide	Content (wt. %)
SiO_2	32.4
MgO	17.90
CaO	17.17
Al_2O_3	7.52
FeO	6.88
K_2O	6.51
P_2O_5	3.75
Na_2O_3	0.40
C	3.04
La	0.01

 doi:10.20944/preprints202504.1931.v1

Ce	0.019
Y	0.002

Table 4. Mineralogical composition of the ore.

Mineral	Content (wt. %)
K-feldspar	2.28
Phlogopite ($KMg_3(AlSi_3O_{10})(OH)_2$)	57.37
Biotite ($K(Mg,Fe)_3(AlSi_3)O_{10}(OH)_2$)	3.18
Apatite ($Ca_5(PO_4)_3(OH, F, Cl)$	8.87
Calcite ($CaCO_3$)	16.68
Dolomite ($CaMg(CO_3)_2$	2.45
Magnetite (Fe_3O_4)	0.74

XRD diagram of the feed is presented in Figure 4. The phases identified through XRD are phlogopite, fluorapatite, calcite and dolomite, which present high content in the sample. It has to be noted that despite the different chemical composition, phlogopite and biotite presents the same XRD peaks, making their discretization impossible through this method. Thus, the different analyses applied for the characterization of the sample are complementary facilitating deeper understanding of the sample composition, and not competitive.

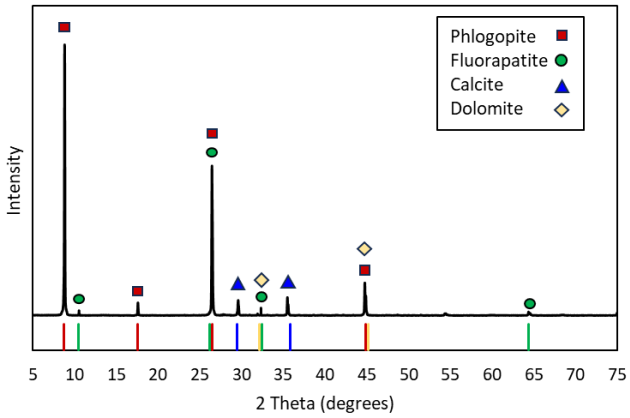

Figure 4. XRD diagram of raw material, and main peaks of identified phases.

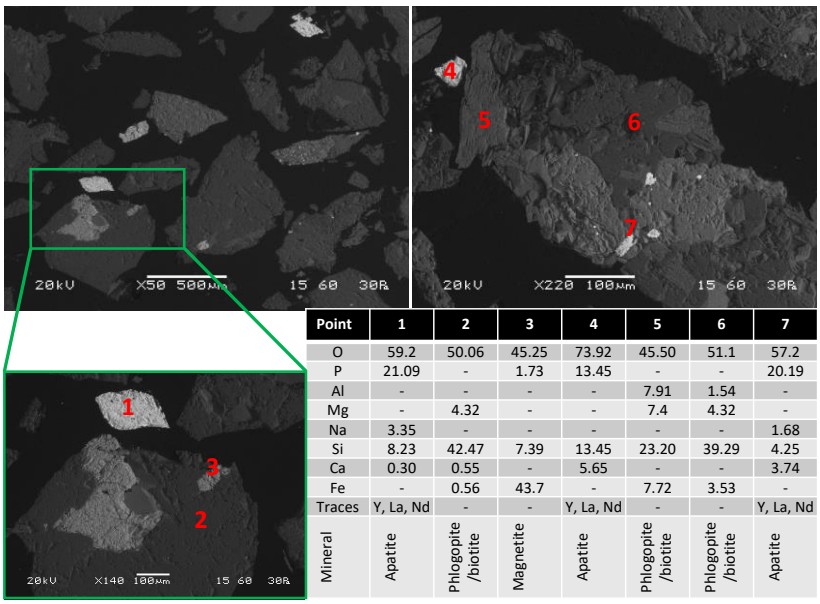

Point	1	2	3	4	5	6	7
O	59.2	50.06	45.25	73.92	45.50	51.1	57.2
P	21.09	-	1.73	13.45	-	-	20.19
Al	-	-	-	-	7.91	1.54	-
Mg	-	4.32	-	-	7.4	4.32	-
Na	3.35	-	-	-	-	-	1.68
Si	8.23	42.47	7.39	13.45	23.20	39.29	4.25
Ca	0.30	0.55	-	5.65	-	-	3.74
Fe	-	0.56	43.7	-	7.72	3.53	-
Traces	Y, La, Nd	-	-	Y, La, Nd	-	-	Y, La, Nd
Mineral	Apatite	Phlogopite /biotite	Magnetite	Apatite	Phlogopite /biotite	Phlogopite /biotite	Apatite

 doi:10.20944/preprints202504.1931.v1

Figure 5. SEM images of the ore thin cuts, combined with EDS analysis for spatial identification of minerals.

Figure 6a depicts sample micrograph with pseudo-colour mapping of particles for easier distinguishing of the identified minerals, while Figure 6b shows grains classified according to the apatite liberation. Phlogopite phase dominates in the raw material, with apatite, calcite and magnetite presence being considerable.

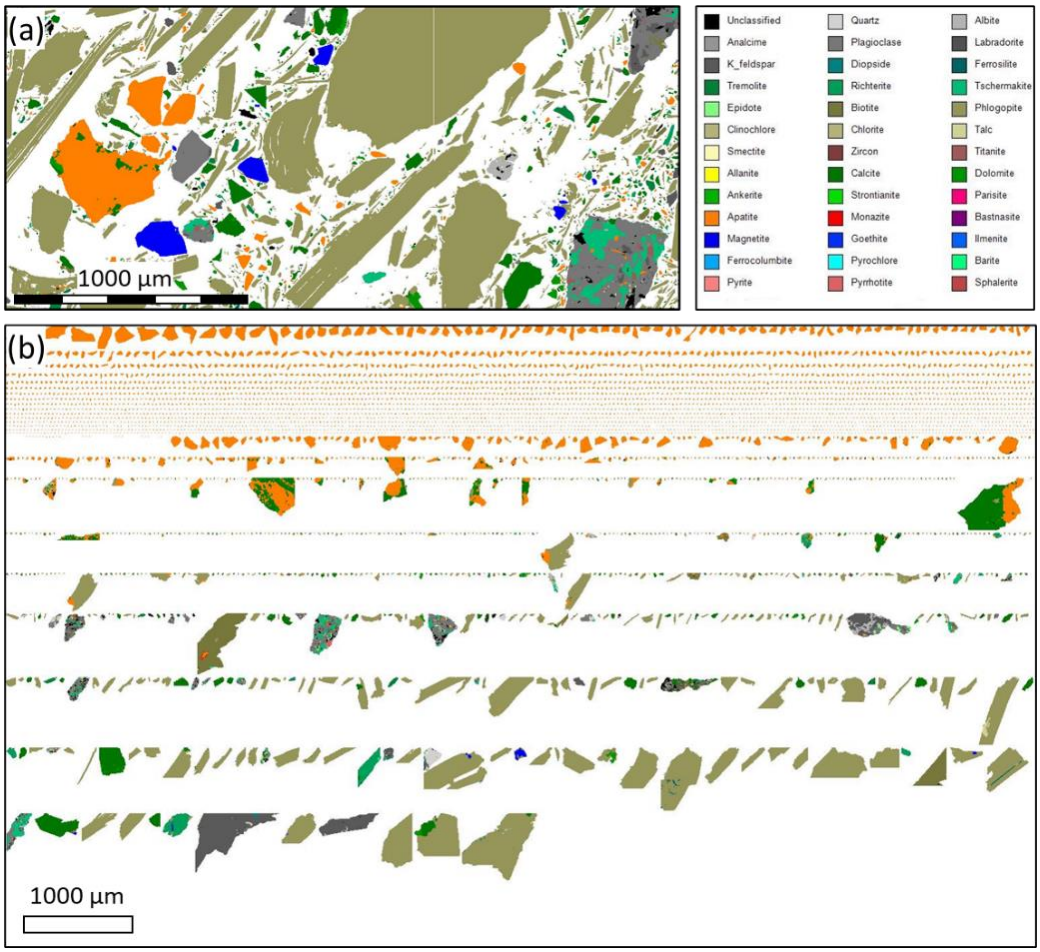

Figure 6. Representative pseudo-colour particle map from the mineral liberation analysis of the ore, and (b) grains classification according to the apatite liberation degree.

Focussing on the REEs, Figure 7a presents grain size for apatite, as well as REE minerals , like parisite($Ca(Ce,La)_2(CO_3)3F_2$), allanite($(Ce,Ca,Y,La)_2(Al,Fe^{+3})_3(SiO_4)_3(OH)$), pyrochlorite ($(Na,Ca)_2Nb_2O_6(OH,F)$), monazite $(Ce,La,Th)PO_4$, zircon ($ZrSiO_4$)and ferrocolumbite ($FeNb_2O_6$). It has to be noted that same phases have been identified by other researchers for this deposit[42] . By considering the size distribution of the liberated apatite grains, which present D80 of 245 µm, and also that all other phases of interest present lower D80 value, grinding process was controlled accordingly. Thus, raw material was grinded for 30 minutes in a laboratory rod mill under wet conditions, and the obtained material reached D80 of 179 µm, and size distribution which is depicted in Figure 8. Elutriation screening was applied for determination of -45 µm grade.

As for the association degree of apatite and REE minerals, presented in Figure 7b, high degree of liberation was identified for allanite, pyrochlorite, apatite and zircon, were the recognized free surfaces exceeded 80 %. Parisite and monazite are equally associated with apatite, calcite and biotite, while ferrocolumbite is solely associated with richterite.

 doi:10.20944/preprints202504.1931.v1

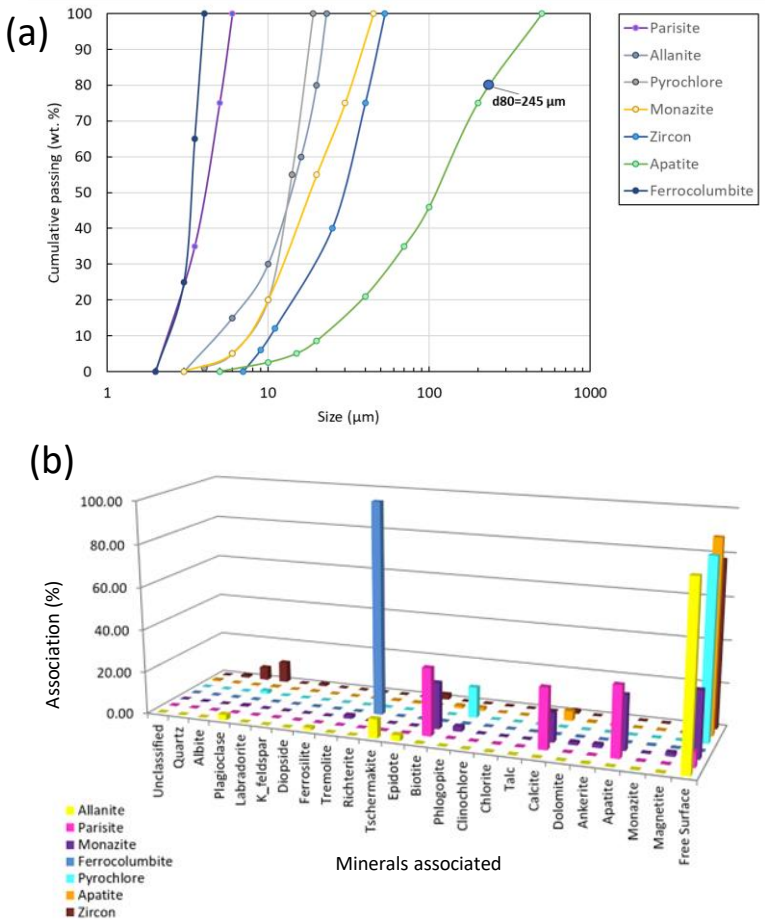

Figure 7. Grains' size distribution for apatite and the identified REE minerals (a), and REE minerals and apatite liberation and association degree with other minerals in the sample.

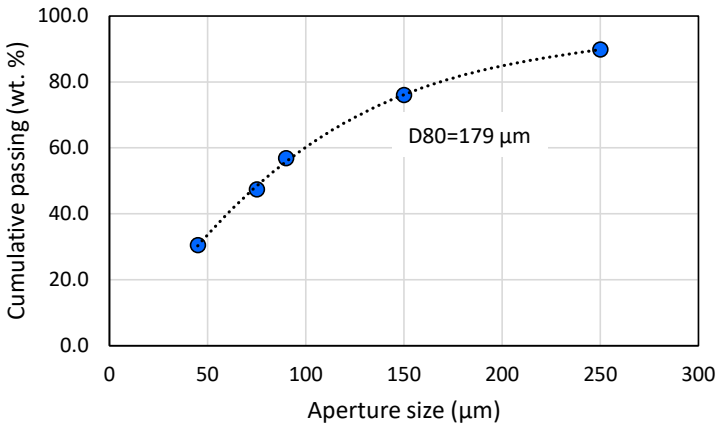

Figure 8. Particle size distribution of the feed after grinding.

The results of the mineralogical analysis of the sample is in line with other published studies that are focused on the geology of the carbonatite complex[14,42,43].

3.2. Lab-Scale Flotation with Conventional Collectors

Figure 9a presents temporal evolution of phosphorus recovery in the concentrates obtained using different collectors, and Figure 9b the evolution of mass pulled (yield) versus the phosphorus recovery. Among the presented flotation trials, higher flotation rates were achieved with

 doi:10.20944/preprints202504.1931.v1

hydroxamate that was dissolved in hot water (55 °C), while the phosphorus recovery reached almost 99% at 9 min of flotation. The selectivity was also adequate as shown in Figure 9b, where the aforementioned recovery reached at mass pull of 34 %.

Such findings are in line with several research highlighting the beneficial effect of heating on the flotation rate, as well on the overall efficiency of hydroxamic collectors. This might be connected to a change in the solubility and activation energy of reagents, the partial dehydration of minerals' surfaces and reagents' molecules, and the removal of ultra fines from the surfaces of the mineral particles[44,45]. Undoubtedly, the increase of the temperature affects hydrodynamics by decreasing the viscosity of the water and increase the rate of elutriation of the gangue back to the pulp [44,46]. However, this is not the case here, since flotation took place under ambient temperature conditions. it is worth noting the work of Pradip and Fuerstenau who investigated the effect of temperate on the adsorption of hydroxamate on minerals like barite, calcite and bastnaesite, and found increased values upon heating suggesting endothermic chemisorption mechanism [47]. Flotation test under elevated temperature confirmed this for monazite and bastnaesite[48,49], as well as apatite and malachite ore [44,50].

As for the use of hydroxamate under ambient conditions, an increase of the reagent dosage increases the flotation rate and the efficiency in general, which however is inadequate for dosage below 250 g/t, where P grade and recovery reached only 80.2% after 9 min of flotation. Sacrosine collector presents the slowest rate in phosphorus collection, however the selectivity is remarkable, with considerable recovery of 89.2 % achieved with mass pull of 16.2%.

 doi:10.20944/preprints202504.1931.v1

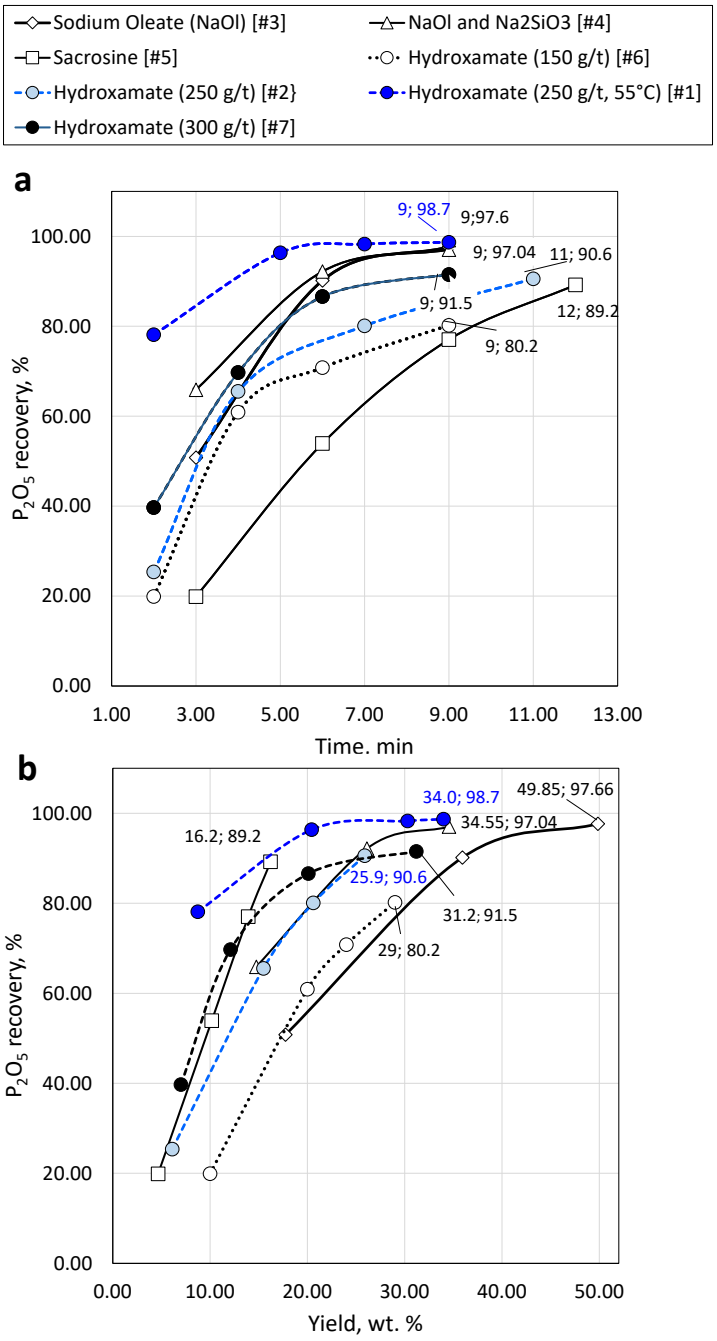

Figure 9. Apatite recovery versus time (a) and mass concentrate yield (b) using different conventional collectors.

The combined concentrates' contents in phosphorus, lanthanum, cerium and yttrium for the aforementioned tests are presented in the graph of Figure 10. A comparison between the results obtained using different reagents reveals that the trend in La, Ce and Y recovery follows that of P; the higher the recovery of apatite the higher is that of REEs, which confirms the characterization findings regarding the apatite hosting of REE minerals.

 doi:10.20944/preprints202504.1931.v1

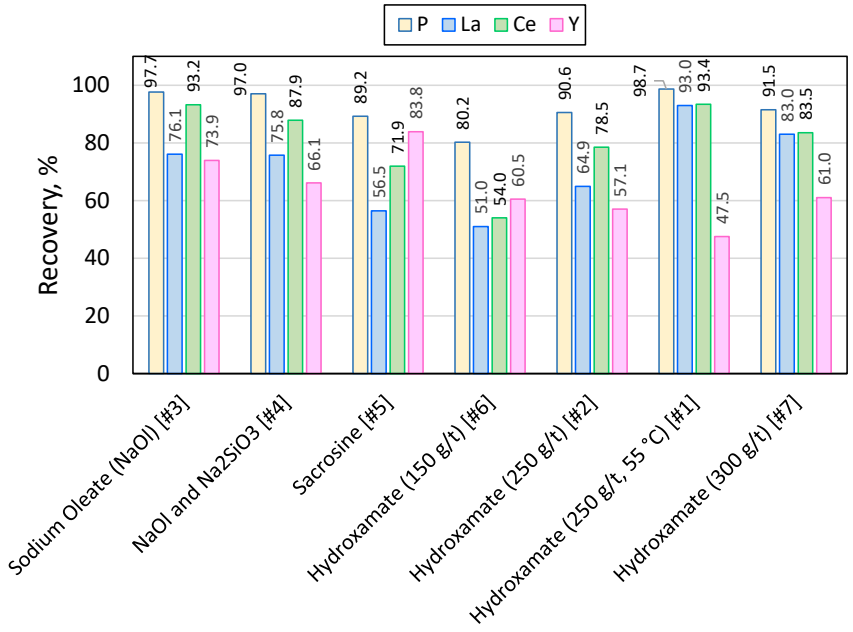

Figure 10. Recovery of phosporus, lantanum, cerrium and ytrium in the combined concentrates for different collectors.

As shown in Table 5, in all cases the concentrate of La, Ce and Y in the produced concentrates exceeded that of the initial ones, with sacrosine and hydroxamate collectors possessing best results.

Table 5. REEs content in the concentrates obtained from the flotation of the ore using conventional reagents. For comparison purposes, the concentration of the elements in the feed are also given in the last raw.

Flotation Experiment	REEs Grade in Final Concentrate, %		
	La	Ce	Y
Sodium Oleate (NaOl) [#3]	0.0192	0.0413	0.0031
NaOl and Na2SiO3 [#4]	0.0237	0.0550	0.0037
Sacrosine [#5]	0.0402	0.0926	0.0054
Hydroxamate (150 g/t) [#6]	0.0498	0.1046	0.0041
Hydroxamate (250 g/t) [#2]	0.0265	0.0627	0.0038
Hydroxamate (250 g/t, 55 °C) [#1]	0.0257	0.0550	0.0032
Hydroxamate (300 g/t) [#7]	0.0299	0.0595	0.0037
In the feed	0.0098	0.0190	0.0020

3.3. Synergy of Lignin with Conventional Reagents

Following the good results of both sacrosine and hydroxamate collectors in terms of the achieved grade and recovery of apatite and the REE of interest (La, Y, Ce) in the concentrate, more flotation trials were carried out applying reduction in collectors 'dosages by 20, 30 and 40 % for sacrosine and 30 and 50 % for hydroxamate and adding lignin nanoparticles, and the respective results are depicted in Figure 11-Figure 14.

More specifically, Figure 11a,b presents apatite recovery versus time, and mass concentrate yield, respectively, using sole sarcosine and sarcosine reduced by 20% and addition of by lignin by 20%, 30% and 40%. Flotation rate increases when 20% reduction of sacrosine is applied, while further increase of reduction ratio by 10% (30% lignin) results in the same flotation rates as with sole sacrosine. When the reduction exceeds 30% further attenuation of the flotation rate is identified. Figure 11b informs about the better selectivity that is achieved when 20% and 30 % sacrosine reduction and lignin nanoparticles addition is applied compared to the two extreme scenarios of sole sacrosine usage or the maximum reduction of 40% and the addition of lignin. Among all trials

 doi:10.20944/preprints202504.1931.v1

presented here, higher phosphorous recovery was achieved at 20% reduction of sacrosine (93.6 %). P, La, Ce and Y recoveries of the combined concentrates are depicted in Figure 12. Except to the Y, the 20% replacement of sacrosine by lignin lead to improvement of P, Ce and La. It is shown here that, for 40% dosage reduction of the specific conventional collector, poor separation efficiency is achieved since the recovery in P as well as in Ce, La and Y are considerably low.

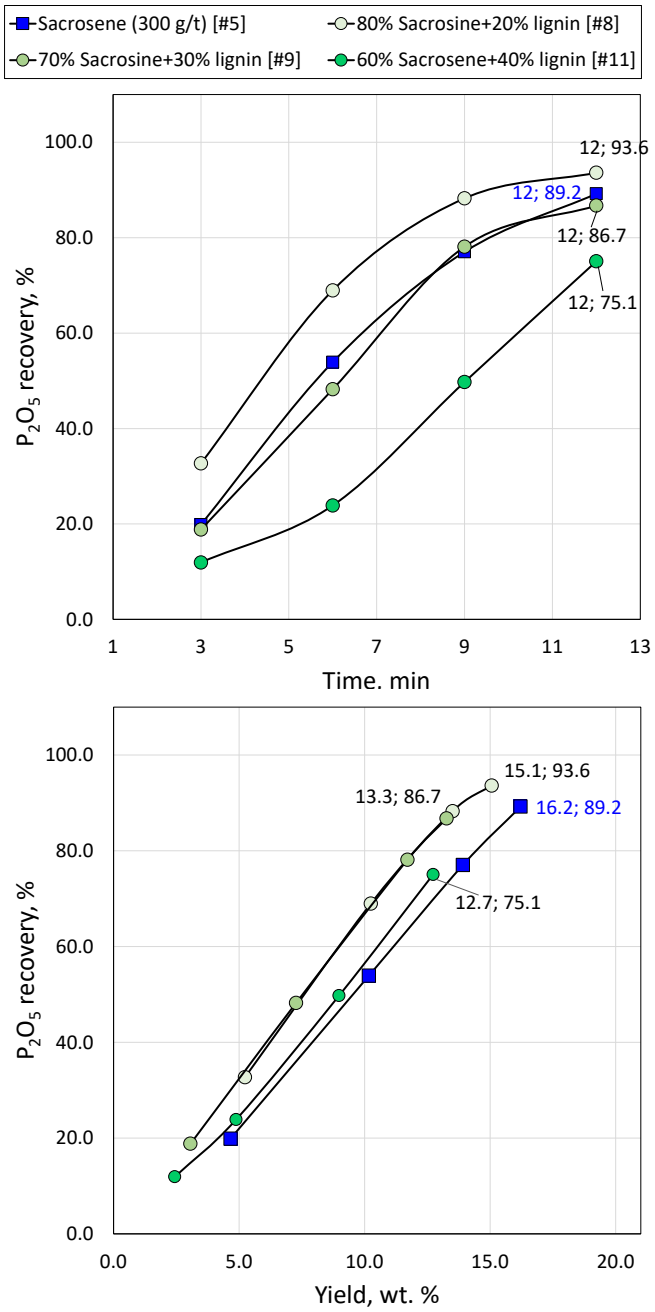

Figure 11. Apatite recovery versus time (a) and mass concentrate yield (b) using sole sarcosine and sarcosine/lignin mixture at different ratio.

 doi:10.20944/preprints202504.1931.v1

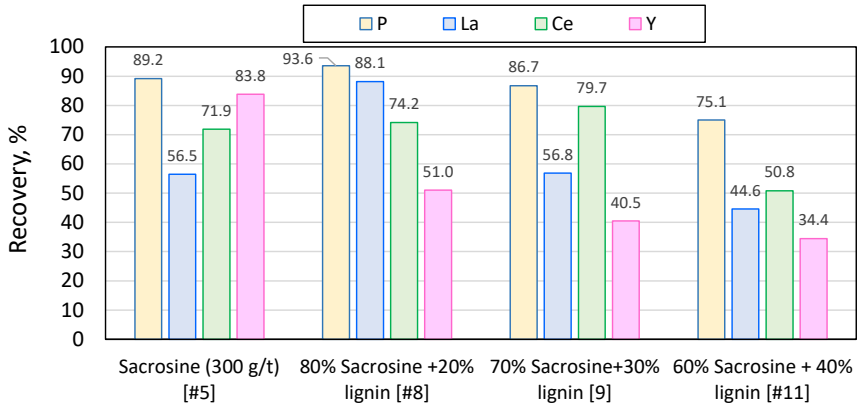

Figure 12. Recovery of phosphorus and major REEs (lanthanum, cerium, yttrium) using solely sarcosine, and sacrosine/lignin mixtures .

Figure 13a,b presents phosphorous recovery versus time and yield, respectively, when sole hydroxamate is used as collector, and for 30% and 50% reduction of hydroxamate and addition of lignin. It appears that the flotation kinetics enhance by 30% reduction of hydroxamate and lignin addition, while flotation rate attenuates by further increase of the lignin content. It is also noteworthy that, almost 4% higher phosphorous recovery is achieved upon 30% reduction of hydroxamate. However, for 50% hydroxamate dosage reduction and addition of lignin, and despite the fact that hydroxamate dosage was 200 g/t, that's is 66% of the control case, the achieved phosphorous recovery reached 86.9% only. As for the effect of collector composition on the selectivity, it appears that, 30% reduction of hydroxamate and addition of lignin is sufficient to achieve higher phosphorous recovery (95.4 %) compared to sole hydroxamate (91.5 %) at similar mass pull (30-31 %). As shown in Figure 14, similar La, Ce and Y recoveries were achieved also in such case, while a reduction in recoveries is observed when dosage reduction is 50 % in all elements of interest.

 doi:10.20944/preprints202504.1931.v1

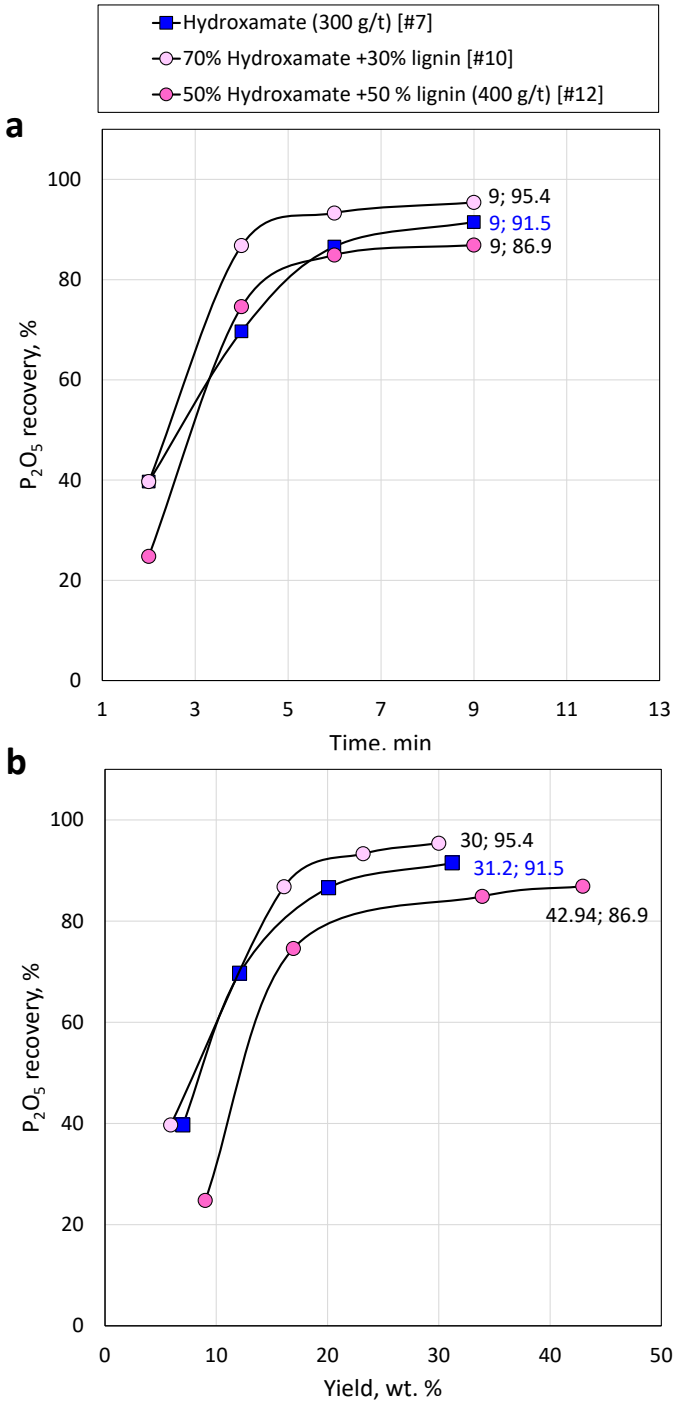

Figure 13. Apatite recovery versus time (a) and mass concentrate yield (b) using sole hydroxamate and hydroxamate/lignin mixture at different ratio.

 doi:10.20944/preprints202504.1931.v1

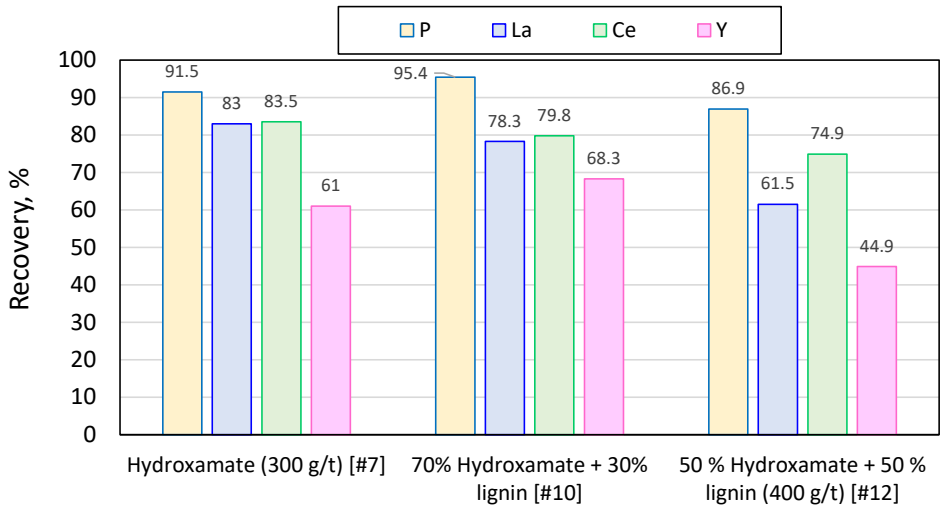

Figure 14. Recovery of phosphorus and major REEs (lanthanum, cerium, yttrium) using solely hydroxamate, and hydroxamate/lignin mixtures .

The FTIR analysis allowed investigation of the interaction between apatite and the reagents, mainly hydroxamate and lignin nanoparticles. Figure 15 depicts FTIR spectra of apatite, lignin nanoparticles and apatite sample treated with sole hydroxamate (300 g/t), hydroxamate (210 g/t) and lignin nanoparticles (90 g/t), and sole lignin nanoparticles (300 g/t) at pH of 10, while Table 6 tabulates characterization of the identified peaks.

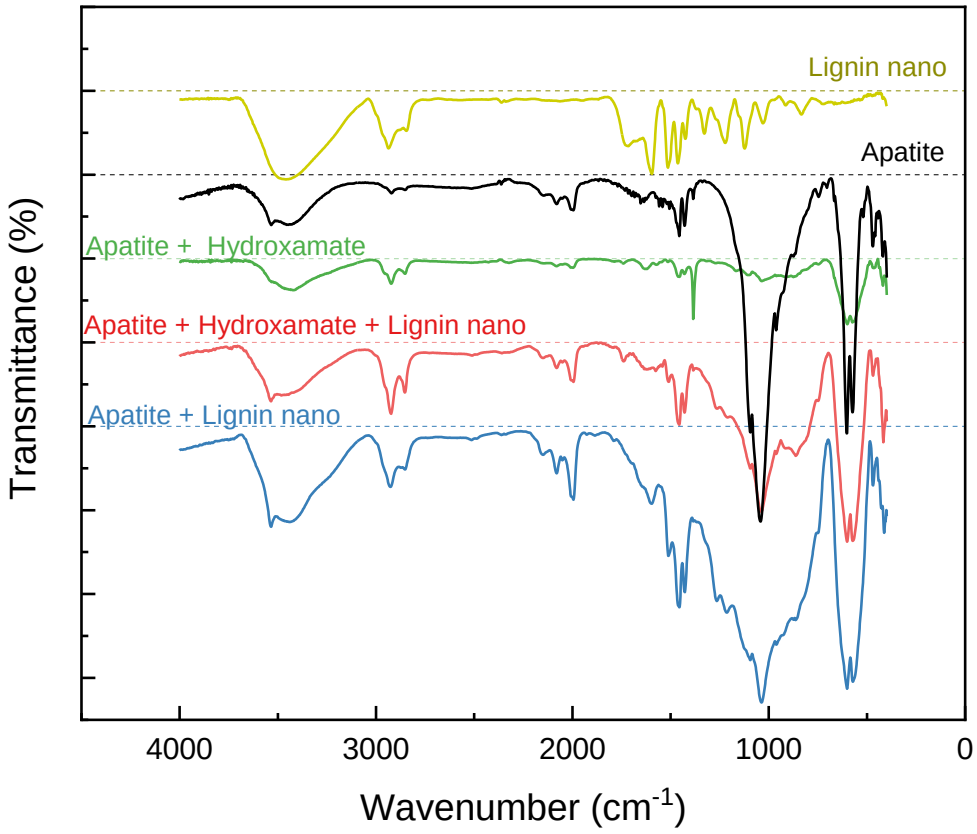

Figure 15. FTIR spectra of apatite and lignin nanoparticles, and apatite treated with sole hydroxamate, hydroxamate and lignin nanoparticles mixture.

 doi:10.20944/preprints202504.1931.v1

There are certain peaks identified in sole apatite and samples treated with lignin, which are at wavenumbers 852 cm^{-1}, 950 cm^{-1}, 1097 cm^{-1}, 2079 cm^{-1} and 3538 cm^{-1} due to C-H deformation of syringyl (S) units, symmetric and asymmetric vibration of PO_4 group and OH vibrations, respectively. Possible interaction of the mineral surface and the lignin nanoparticles might be indicated by the peak at 1512cm^{-1}, which appears only when apatite and lignin nanoparticles come together, while is not present in the individual phases. Interestingly the peak did not appear in sole apatite or lignin, although would be expected to the organic sample since it is attributed to C=C aromatic skeletal vibration. Also, new peaks identified after using lignin in the collector mixture are at 1214 cm^{-1} and 1326 cm^{-1} attributed to absorbance of guaiacyl and C=O bending of syringyl unit, both of which are structural components of lignin [51].

Possible interaction of apatite with either hydroxamate and/or lignin nanoparticles should be accompanied by change in the intensity or shifting of peaks associated to hydroxyl (-OH), carbonyl (C=O), or phosphate PO_4 functional groups. Although no peak shifting was identified, however, in most cases, all peaks related to the aforementioned functional groups appear enhanced after the interaction of the mineral with hydroxamate and lignin, except to the wide peak at 1000-1150 cm^{-1} associated with asymmetric stretching of PO_4 which attenuated after the addition of hydroxamate, however remains strong after the use of hydroxamate-lignin mixture. Also, enhancement of OH peak at 3538 cm^{-1} occurred after the treatment of apatite with hydroxamate and lignin nanoparticles, that might denote interaction of the species. Such findings provide indications of interaction of apatite with lignin through hydrogen bonding, but a more focused study is required to provide insights regarding the interaction mechanism, involved functional groups and bond type.

Table 6. FTIR peaks identified under apatite treatment with sole hydroxamate, hydroxamate and lignin nanoparticles mixture and sole lignin nanoparticles.

Wavelength (cm^{-1})	Mode	Apatite	Lignin nano	Apatite + Hydroxamate	Apatite + Hydroxamate + Lignin nano	Apatite + Lignin nano	Reference
		Intensity (w: weak, m: medium, s: strong)					
468	Deformation vibration of P-O	**m**	**-**	**w**	**w**	m	[36,52]
573		m	-	w	m	m	[52,53]
600		m	-	w	m	m	[52,53]
742	OH vibration band	w	-	w	w	w	[54]
853	C-H out-of-plane deformation of syringyl (S) unit	w	m	-	m	m	[55]
956	Symmetric stretching of PO_4 group	w	-	-	w	w	[54]
1021	Aromatic C-H in plane deformation for S units	s	-	w	s	s	[36]
1000-1150	Asymmetric stretching of the PO_4 group	s	-	w	s	s	[53,54]
1214	Absorbance of guaiacyl	-	m	-	w	w	[36]
1326	C=O bending of S unit	-	m	-	w	w	[36]

 doi:10.20944/preprints202504.1931.v1

1385	OH vibration band	w	-	s	-	-	[54]
1460	C-H bending	m	-	w	m	s	[36]
1512	C=C aromatic skeletal vibration		-	-	w	w	[36]
1590			-	w	-	m	[36]
1623	C=N stretching	w	-	m	w	-	[56]
1999	PO_4	m	-	w	m	s	[54]
2079	PO_4	w	-	-	w	m	[54]
2855	C-H stretching in $-CH_2$ and $-CH_3$	w	-	w	m	w	[36]
2926		w	-	w	s	m	
3420	O-H stretching	w	-	w	w	m	[36]
3538	OH vibration band	w	-	-	w	m	[54]

The contact angles of apatite and phlogopite when exposed to hydroxamate and a combination of hydroxamate and lignin under pH of 10 are presented in Figure 16. After being treated with hydroxamate (300 g/t), apatite and phlogopite presented contact angle values of 79.6 ° and 53.8 °, respectively. After minerals treatment with hydroxamate (210 g/t) and lignin (90 g/t), apatite presents contact angle value of 75.2 °, which is slightly lower compared to the case of treatment with sole Aero. This is not the case for phlogopite, which presented a significantly reduced contact angle value of 36.9° in case of lignin addition. The results suggest that the adsorption of lignin on phlogopite was greater than on apatite, enhancing the hydrophilicity of the mineral, thus inhibiting its flotation.

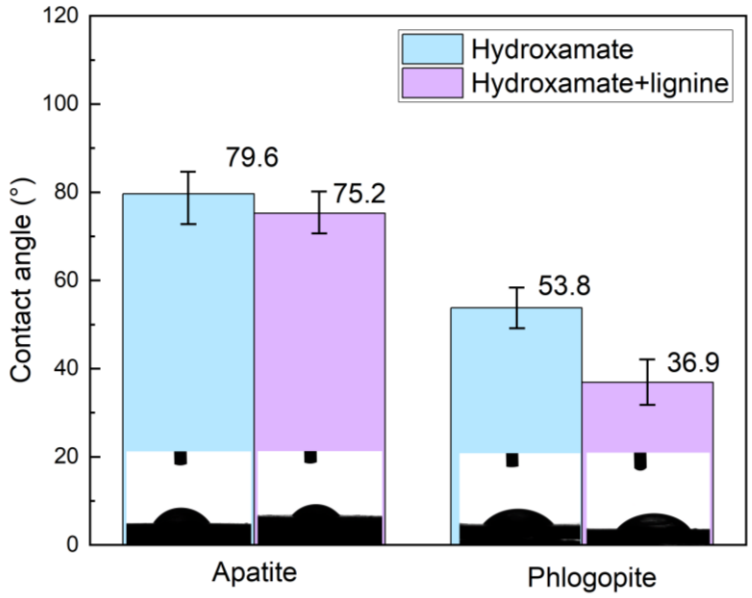

Figure 16. Contact angle of single minerals treated using different chemicals.

3.4. Separation Efficiency

Further evaluation of the flotation results was done using two flotation indexes. The Selectivity Index (SI) is calculated from Equation 1 [57]:

$$SI = \sqrt{\frac{R_{v,c} * R_{g,t}}{(100 - R_{v,c}) * (100 - R_{g,t})}} \quad (1)$$

where $R_{v,c}$ and $R_{g,t}$ are the recovery of the valuable in the concentrate and of the gangue in the tailings, respectively. SI value over 1 denotes selectivity in flotation of the valuable over the gangue, however,

 doi:10.20944/preprints202504.1931.v1

higher values are desirable. In our case, phlogopite is considered the gangue mineral and Mg is the tracer element.

The Separation Efficiency (SE) is calculated by [58]:

$$SE = R_{v,c} - R_{g,c} \quad (2)$$

where $R_{g,t}$ is the recovery of gangue in the concentrate. SE value over 80% reflects excellent separation.

Table 7 tabulates recoveries of phosphorous in concentrate, and of magnesium in concentrate and tailings, as well selectivity index and separation efficiency for all lad-scale flotation tests (conditions are presented in

Table 7 P and Mg distribution in concentrates and tailings, and SI and SE values for all laboratory flotation tests.

Number.	Reagents	Conv. collector Replacement (%)	P recovery in Conc. (%)	Mg recovery in Conc. (%)	Mg recovery in Tail (%)	Selectivity Index	Separation efficiency
1	Hydroxamate diluted at 55 °C	-	98.7	13.6	86.4	5.2	85.1
2	Hydroxamate	-	90.6	13.7	86.3	0.7	76.9
3	Fatty acid	-	97.7	38.3	61.7	0.9	59.4
4	Fatty acid, Na_2SiO_3	-	97	46.2	53.8	0.5	50.8
5	Sacrosine	-	89.2	6.7	93.3	1.3	82.5
6	Hydroxamate, Na_2SiO_3	-	80.2	59.3	40.7	0.0	20.9
7	Hydroxamate, Na_2SiO_3	-	91.5	8.9	91.1	1.2	82.6
8	Sacrosine, lignin	20	93.6	4.8	95.2	3.1	88.8
9	Sacrosine, lignin	30	86.7	5.5	94.5	1.2	81.2
10	Hydroxamate, lignin, Na_2SiO_3	30	95.4	18.6	81.4	1.0	76.8
11	Sacrosine, lignin	40	75.1	4.7	95.3	0.7	70.4
12	Hydroxamate, lignin, Na_2SiO_3	50	86.9	5.9	94.1	1.2	81

As far as the selectivity index, the highest value is reached when hydroxamate is used as collector, which prior have been diluted in aqueous solution preheated at 55 °C. A 80/20 v/v sacrosine/lignin collector mixture performed very well too, which further to the high selective index (3.1) exhibits the highest separation efficiency (88.8%). When replacement ratio of both sarcosine and hydroxamate by lignin exceeds 30 %, the flotation performance declines, which is reflected by low phosphorous and/high magnesium recoveries in concentrate or by low selectivity index and separation efficiency.

3.5. Bench-Scale Flotation Tests

Figure 17a and Figure 17b presents grade and recovery curves for P and for La and Ce, respectively, using 4 and 13 L flotation cell and sole sacrosine and sacrosine/lignin 80/20 mixture collectors. Satisfactory phosphorous recovery of 95.3 % and 96,5 % is observed when sole sacrosine and sacrosine/lignin was used in 4L cell, respectively. The respective P grade was found 17.4 % and 19.1 %. Better flotation results are obtained by process upscaling in 13L cell; in that case, the P grade and recovery reached 24.2% and 94.5 %, respectively. As for the lanthanum and cerium content, the achieved cumulative Ce and La grade and recovery for sole sacrosine is 0.12% and 73.3%, respectively, and for sacrosine/lignin is 0.13% and 77.8% in 4L cell. Thus, the partial replacement of sacrosine by lignin allows increase of the recovery by about 4.5% at the same grade. Upon increase

 doi:10.20944/preprints202504.1931.v1

of the flotation cell size, the La and Ce grade in the concentrate increases at 0.15% at the expense of recovery which falls to 71.2 %.

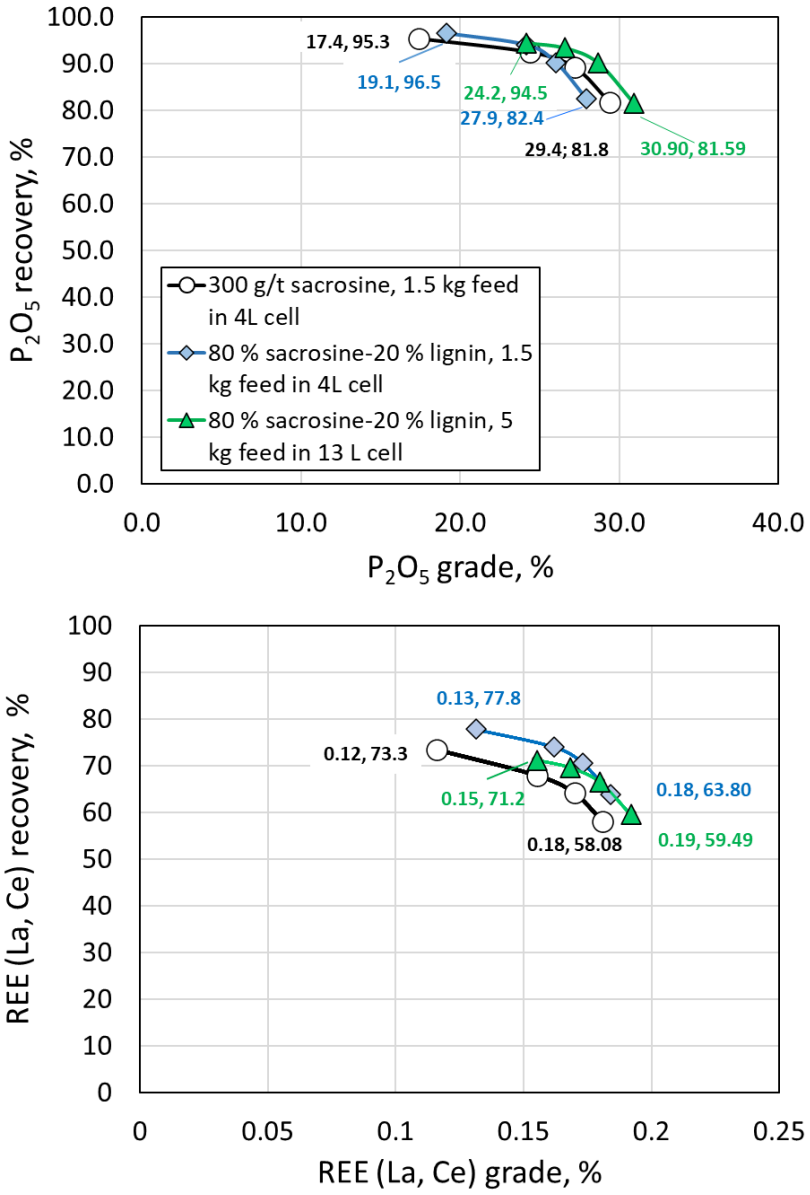

Figure 17. Phosphorous, and Lanthanium and Cerrium grade and recovery using solely sacrosin in lab scale trials, and 80/20 sacrosine/lignin mixture in lab and bench scale trials with 4 and 13 L cell size and 1.5 kai and 5 kg feed, respectively.

4. Conclusions

The study presented the results of flotation tests for the recovery of REE-hosting apatite from ore originating from a carbonatite deposit, Finland, using conventional anionic and amine-based collectors, but also natural organosolv lignin nanoparticles individually or a mixture to identify synergies. The following conclusions are drawn from the chemical and mineralogical characterization of the ore, and the evaluation of flotation products:

The ore originates from carbonatite deposit, located in central Finland exhibits fluorapatite content of about 8.9 %, having also overall content on L, Ce and Y of about 0.03%.

Apatite hosts most of REE minerals, which was confirmed by the flotation tests which shown that the concentration of apatite implies concentration of the L, Ce and Y.

 doi:10.20944/preprints202504.1931.v1

Adequate recovery of apatite and REEs was achieved using common anionic collectors hydroxamate and sacrosine reaching P grade of 23.4 and 21.5%, and recovery of 96.4% and 89.2 %, at collector dosage of 250 and 300 g/t, and pH of 10 and 11, respectively.

The reduction of conventional collectors by up to 30% and the addition of lignin nanoparticles does not burden the flotation process and does not deteriorate the quality of the concentrate; in sacrosine and hydroxamate after collectors' reduction by 30% and addition of lignin nanoparticles the P recovery reached 86.7% and 95.4 %, respectively.

Bench scale flotation tests in 13 L flotation cell confirmed the lab-scale results for sacrosine; 20 % reduction of sacrosine and addition of lignin nanoparticles allowed obtaining of concentrate with P recovery of 94.5%, and La and Ce recovery of 71.5%.

The enhancement of FT-IR peaks related to PO_4 and OH species when apatite was treated with lignin nanoparticles indicate interaction of species possibly through hydrogen bonding, however a focused study is needed to confirm this and gain more insights regarding bonding type.

Lignin appears to increase the hydrophilicity of both apatite and phlogopite, with the effect being more pronounced in the latter, thereby improving their separation via flotation.

Author Contributions: For research articles with several authors, a short paragraph specifying their individual contributions must be provided. The following statements should be used "Conceptualization, P.M.A, X.S.Y, G.A and P.C.; methodology, P.M.A., X.S.Y and G.A; investigation, P.M.A., X.S.Y. and N.K.; resources, P.C, X.S.Y and M.T; writing—original draft preparation, P.M.A; writing—review and editing, P.M.A.; supervision, P.C and M.T; funding acquisition, P.C., X.S.Y and M.T. All authors have read and agreed to the published version of the manuscript.".

Funding: This research has received funding from the EIT Raw Materials research and innovation programme under Proposal Number n◦19392, project "BAT-PLUS. INCREASE of supply of BATTERy minerals by FLotAtIon of REE-rich apatite".

Data Availability Statement: Data are contained within the article.

Conflicts of Interest: The authors declare no conflicts of interest.

References

1. Moldoveanu, G.A.; Papangelakis, V.G. Recovery of Rare Earth Elements Adsorbed on Clay Minerals: I. Desorption Mechanism. *Hydrometallurgy* **2012**, *117–118*, 71–78, doi:10.1016/j.hydromet.2012.02.007.
2. Mokoena, B.K.; Mokhahlane, L.S.; Clarke, S. Effects of Acid Concentration on the Recovery of Rare Earth Elements from Coal Fly Ash. *Int. J. Coal Geol.* **2022**, *259*, 104037, doi:10.1016/j.coal.2022.104037.
3. Dushyantha, N.P.; Ratnayake, N.P.; Premasiri, H.M.R.; Ilankoon, I.M.S.K.; Hemalal, P.V.A.; Jayawardena, C.L.; Chandrajith, R.; Rohitha, L.P.S.; Abeysinghe, A.M.K.B.; Dissanayake, D.M.D.O.K.; et al. Leaching of Rare Earth Elements (REEs) from Lake Sediments around Eppawala Phosphate Deposit, Sri Lanka: A Secondary Source for REEs. *Hydrometallurgy* **2021**, *205*, 105751, doi:10.1016/j.hydromet.2021.105751.
4. Cordier, D. U.S. Geological Survey, 2023, Rare Earths Available online: https://pubs.usgs.gov/periodicals/mcs2024/mcs2024-molybdenum.pdf (accessed on 7 September 2024).
5. Goodenough, K.M.; Schilling, J.; Jonsson, E.; Kalvig, P.; Charles, N.; Tuduri, J.; Deady, E.A.; Sadeghi, M.; Schiellerup, H.; Müller, A.; et al. Europe's Rare Earth Element Resource Potential: An Overview of REE Metallogenetic Provinces and Their Geodynamic Setting. *Ore Geol. Rev.* **2016**, *72*, 838–856, doi:https://doi.org/10.1016/j.oregeorev.2015.09.019.
6. EuRare Project Webpage Available online: https://www.eurare.org/contactUs.html (accessed on 14 November 2024).
7. Bhattacharjee, M.; Behera, K.K.; Swain, S.P. Apatite-Hosted REE Mineralization in the Eastern Ghats Mobile Belt: A Future Prospect for REE. *Geosystems and Geoenvironment* **2024**, *3*, 100290, doi:https://doi.org/10.1016/j.geogeo.2024.100290.

 doi:10.20944/preprints202504.1931.v1

8. Owens, C.L.; Nash, G.R.; Hadler, K.; Fitzpatrick, R.S.; Anderson, C.G.; Wall, F. Apatite Enrichment by Rare Earth Elements: A Review of the Effects of Surface Properties. *Adv. Colloid Interface Sci.* **2019**, *265*, 14–28, doi:10.1016/j.cis.2019.01.004.
9. Xiqiang, L.; Hui, Z.; Yong, T.; Yunlong, L. REE Geochemical Characteristic of Apatite: Implications for Ore Genesis of the Zhijin Phosphorite. *Minerals* 2020, *10*.
10. Ihlen, P.M.; Schiellerup, H.; Gautneb, H.; Skår, Ø. Characterization of Apatite Resources in Norway and Their REE Potential — A Review. *Ore Geol. Rev.* **2014**, *58*, 126–147, doi:https://doi.org/10.1016/j.oregeorev.2013.11.003.
11. Hughes, J.M.; Cameron, M.; Mariano, A.N. Rare-Earth-Element Ordering and Structural Variations in Natural Rare-Earth-Bearing Apatites. *Am. Mineral.* **1991**, *76*, 1165–1173.
12. Pan, Y.; Fleet, M.E. Compositions of the Apatite-Group Minerals: Substitution Mechanisms and Controlling Factors. *Rev. Mineral. Geochemistry* **2002**, *48*, 13–49, doi:10.2138/rmg.2002.48.2.
13. O'Brien, H.; Heilimo, E.; Heino, P. Chapter 4.3 - The Archean Siilinjärvi Carbonatite Complex. In; Maier, W.D., Lahtinen, R., O'Brien, H.B.T.-M.D. of F., Eds.; Elsevier, 2015; pp. 327–343 ISBN 978-0-12-410438-9.
14. Decrée, S.; Savolainen, M.; Mercadier, J.; Debaille, V.; Höhn, S.; Frimmel, H.; Baele, J.M. Geochemical and Spectroscopic Investigation of Apatite in the Siilinjärvi Carbonatite Complex: Keys to Understanding Apatite Forming Processes and Assessing Potential for Rare Earth Elements. *Appl. Geochemistry* **2020**, *123*, doi:10.1016/j.apgeochem.2020.104778.
15. Puustinen, K.; Kauppinen, H. The Siilinjärvi Carbonatite Complex, Eastern Finland. In *Phosphate deposits of the world. Volume 2: phosphate rock resources*; A. J. G. Notholt D. F. Davidsoneditors, R.P.S., Ed.; Cambridge University Press, 1989; pp. 394–397 ISBN 0-521-67333-X PP - Cambridge.
16. Al Ani, T. *Mineralogy and Petrography of Siilinjärvi Carbonatite and Glimmerite Rocks, Estern Finland*; 2013;
17. Vaziri Hassas, B.; Rezaee, M.; Pisupati, S. V Precipitation of Rare Earth Elements from Acid Mine Drainage by CO2 Mineralization Process. *Chem. Eng. J.* **2020**, *399*, 125716, doi:https://doi.org/10.1016/j.cej.2020.125716.
18. Patil, A.B.; Struis, R.P.W.J.; Ludwig, C. Opportunities in Critical Rare Earth Metal Recycling Value Chains for Economic Growth with Sustainable Technological Innovations. *Circ. Econ. Sustain.* **2023**, *3*, 1127–1140, doi:10.1007/s43615-022-00204-7.
19. Jordens, A.; Cheng, Y.P.; Waters, K.E. A Review of the Beneficiation of Rare Earth Element Bearing Minerals. *Miner. Eng.* **2013**, *41*, 97–114, doi:https://doi.org/10.1016/j.mineng.2012.10.017.
20. Yang, X.; Heino, N.; Pakkanen, L. Beneficiation Studies of a Rare Earth Ore from the Olserum Deposit. *Nat. Resour.* **2019**, *10*, 346–357, doi:10.4236/nr.2019.109023.
21. Alsabbagh, A.H.; Mustafa, R.M. Wet Gravity Separation and Froth Floatation Techniques for Rare Earth Elements Beneficiation from Monazite Ore in Jordan. *Heliyon* **2023**, *9*, e19597, doi:https://doi.org/10.1016/j.heliyon.2023.e19597.
22. Quast, K. Flotation of Hematite Using C6-C18 Saturated Fatty Acids. *Miner. Eng.* **2006**, *19*, 582–597, doi:10.1016/j.mineng.2005.09.010.
23. Li, D.; Nie, G.; Wang, Z.; Li, J.; Li, J. Flotation Separation of Dolomite from Fluorapatite Using NaF as an Activator. *Surf. Interface Anal.* **2021**, *53*, 860–866, doi:https://doi.org/10.1002/sia.6988.
24. Jong, K.; Han, Y.; Ryom, S. Flotation Mechanism of Oleic Acid Amide on Apatite. *Colloids Surfaces A Physicochem. Eng. Asp.* **2017**, *523*, 127–131, doi:https://doi.org/10.1016/j.colsurfa.2016.11.038.
25. Eskanlou, A.; Arnold, B.J.; Foucaud, Y.; Badawi, M.; Dzade, N.Y. Optimizing Flotation Separation of Fluorapatite from Florida Waste Clay Using a Multiscale Approach. *Appl. Surf. Sci.* **2024**, *662*, 160067, doi:https://doi.org/10.1016/j.apsusc.2024.160067.
26. Karlkvist, T.; Patra, A.; Rao, K.H.; Bordes, R.; Holmberg, K. Flotation Selectivity of Novel Alkyl Dicarboxylate Reagents for Apatite–Calcite Separation. *J. Colloid Interface Sci.* **2015**, *445*, 40–47, doi:https://doi.org/10.1016/j.jcis.2014.11.072.
27. Zheng, H.; Chen, Y.; Weng, X.; Jin, Y.; Kasomo, R.M.; Ao, S. Flotation Separation of Dolomite from Fluorapatite Using Sodium Dodecyl Benzene Sulfonate as the Efficient Collector under Low Temperature. *Minerals* 2022, *12*.

 doi:10.20944/preprints202504.1931.v1

28. Wang, L.; Tian, M.; Khoso, S.A.; Hu, Y.; Sun, W.; Gao, Z. Improved Flotation Separation of Apatite from Calcite with Benzohydroxamic Acid Collector. *Miner. Process. Extr. Metall. Rev.* **2019**, *40*, 427–436, doi:10.1080/08827508.2019.1666126.
29. Paulsen Thoresen, P.; Lange, H.; Crestini, C.; Rova, U.; Matsakas, L.; Christakopoulos, P. Characterization of Organosolv Birch Lignins: Toward Application-Specific Lignin Production. *ACS Omega* **2021**, *6*, 4374–4385, doi:10.1021/acsomega.0c05719.
30. Hrůzová, K.; Kolman, K.; Matsakas, L.; Nordberg, H.; Christakopoulos, P.; Rova, U. Characterization of Organosolv Lignin Particles and Their Affinity to Sulfide Mineral Surfaces. *ACS Appl. Nano Mater.* **2023**, *6*, 17387–17396, doi:10.1021/acsanm.3c02069.
31. Qian, H.; Bao, J.; Shen, C.; Wu, D.; Wang, J.; Hao, H.; Zhang, Y. Improved Flotation Separation of Scheelite from Calcite by Sulfomethylated Kraft Lignin. *Materials (Basel).* **2023**, *16*, doi:10.3390/ma16134690.
32. Vidal, C.; Carrillo-Varela, I.; Reyes-Contreras, P.; Gutiérrez, L.; Mendonça, R.T. Sulfomethylation of Radiata Pine Kraft Lignin and Its Use as a Molybdenite Depressant in Selective Chalcopyrite-Molybdenite Separation by Flotation. *Bioresources* **2021**, *16*, 5646–5666, doi:10.15376/biores.16.3.5646-5666.
33. Hrůzová, K.; Matsakas, L.; Sand, A.; Rova, U.; Christakopoulos, P. Organosolv Lignin Hydrophobic Micro- and Nanoparticles as a Low-Carbon Footprint Biodegradable Flotation Collector in Mineral Flotation. *Bioresour. Technol.* **2020**, *306*, 123235, doi:10.1016/j.biortech.2020.123235.
34. Witecki, K.; Szkurat, M.; Hruzova, K. Organosolv Lignin Particles as an Ecological Reagent in the Kupfershiefer Copper Ore Flotation. *Physicochem. Probl. Miner. Process.* **2023**, *59*, 174363, doi:10.37190/PPMP/174363.
35. Angelopoulos, P.M.; Anastassakis, G.; Kountouris, N.; Taxiarchou, M.; Koutsotheodorou, E.; Pefkos, T.; Klepkos, V.; Samara, C.; Mprokos, G. Flotation of Sulphide Minerals Using Organosolv Lignin as Collector—Pilot-Scale Trials. *Mater. Proc.* 2023, *15*.
36. Bazar, J.A.; Hrůzová, K.; Jolsterå, R.; Matsakas, L.; Rova, U.; Christakopoulos, P. Enhancing Froth Flotation Performance of Iron Oxide Apatite Ore Tailings through Synergistic Utilization of Organosolv Lignin Particles and Tall Oil Fatty Acid-Based Collector. *Miner. Eng.* **2024**, *216*, 108868, doi:https://doi.org/10.1016/j.mineng.2024.108868.
37. Kalogiannis, K.G.; Matsakas, L.; Aspden, J.; Lappas, A.A.; Rova, U.; Christakopoulos, P. Acid Assisted Organosolv Delignification of Beechwood and Pulp Conversion towards High Concentrated Cellulosic Ethanol via High Gravity Enzymatic Hydrolysis and Fermentation. *Molecules* **2018**, *23*, 1–18, doi:10.3390/molecules23071647.
38. Matsakas, L.; Gerber, M.; Yu, L.; Rova, U.; Christakopoulos, P. Preparation of Low Carbon Impact Lignin Nanoparticles with Controllable Size by Using Different Strategies for Particles Recovery. *Ind. Crops Prod.* **2020**, *147*, 112243, doi:10.1016/j.indcrop.2020.112243.
39. Valderrama, L.; Gómez, O.; Pavez, O.; Santander, M. Recovery of Apatite from Magnetic Concentration Tailings by Flotation. *Minerals* **2024**, *14*, doi:10.3390/min14050441.
40. Pålsson, B.I.; Martinsson, O.; Wanhainen, C.; Fredriksson, A. Unlocking Rare Earth Elements from European Apatite-Iron Ores. *1st Eur. Rare Earth Resour. Conf.* **2014**, 211–220.
41. Karlkvist, T. Selectivity in Calcium Mineral Flotation - An Analysis of Novel and Existing Approaches, Lulea University of Technology, 2017.
42. Karvinen, S.; Heinonen, A.; Beier, C.; Jöns, N. The Composition of Apatite in the Archean Siilinjärvi Glimmerite-Carbonatite Complex in Eastern Finland. *Bull. Geol. Soc. Finl.* **2024**, *96*, 1–29, doi:10.17741/bgsf/96.1.001.
43. Salo, A. Geology of the Jaakonlampi Area in the Siilinjärvi Carbonatite Complex. **2016**, 27.
44. Su, F.; Hanumantha Rao, K.; Forssberg, K.S.E.; Samskog, P.O. The Influence of Temperature on the Kinetics of Apatite Flotation from Magnetite Fines. *Int. J. Miner. Process.* 1998, *54*, 131–145.
45. Cooke, S.R.B.; Iwasaki, I.; Choi, H.. Effect of Temperature in Soap Flotation of Iron Ore. *Trans. AIME* **1960**, 76–83.
46. O'Connor, C.T.; Mills, P.J.T. The Effect of Temperature on the Pulp and Froth Phases in the Flotation of Pyrite. *Miner. Eng.* 1990, *3*, 615–624.

 doi:10.20944/preprints202504.1931.v1

47. Pradip; Fuerstenau, D.W. Adsorption of Hydroxamate Collectors on Semi-Soluble Minerals Part II: Effect of Temperature on Adsorption. *Colloids and Surfaces* 1985, *15*, 137–146.
48. Li, M.; Gao, K.; Zhang, D.; Duan, H.; Ma, L.; Huang, L. The Influence of Temperature on Rare Earth Flotation with Naphthyl Hydroxamic Acid. *J. Rare Earths* **2018**, *36*, 99–107.
49. Pavez, O.; Peres, A.E.C. Effect of Sodium Metasilicate and Sodium Sulphide on the Floatability of Monazite-Zircon-Rutile with Oleate and Hydroxamates. *Miner. Eng.* 1993, *6*, 69–78.
50. Marion, C.; Jordens, A.; Li, R.; Rudolph, M.; Waters, K.E. An Evaluation of Hydroxamate Collectors for Malachite Flotation. *Sep. Purif. Technol.* **2017**, *183*, 258–269, doi:https://doi.org/10.1016/j.seppur.2017.02.056.
51. Sammons, R.J.; Harper, D.P.; Labbe, N.; Bozell, J.J.; Elder, T.; Rials, T.G. Characterization of Organosolv Lignin Using Thermal and FT-IR Spectroscopic Analysis. *Bioresources* **2013**, *8*, 2752–2767.
52. Yang, B.; Yin, W.; Zhu, Z.; Sun, H.; Sheng, Q.; Fu, Y.; Yao, J.; Zhao, K. Differential Adsorption of Hydrolytic Polymaleic Anhydride as an Eco-Friendly Depressant for the Selective Flotation of Apatite from Dolomite. *Sep. Purif. Technol.* **2021**, *256*, 117803, doi:https://doi.org/10.1016/j.seppur.2020.117803.
53. Balan, E.; Delattre, S.; Roche, D.; Segalen, L.; Morin, G.; Guillaumet, M.; Blanchard, M.; Lazzeri, M.; Brouder, C.; Salje, E.K.H. Line-Broadening Effects in the Powder Infrared Spectrum of Apatite. *Phys. Chem. Miner.* **2011**, *38*, 111–122, doi:10.1007/s00269-010-0388-x.
54. Nunes, A.P.L.; Peres, A.E.C.; Chaves, A.P.; Ferreira, W.R. Effect of Alkyl Chain Length of Amines on Fluorapatite and Aluminium Phosphates Floatabilities. *J. Mater. Res. Technol.* **2019**, *8*, 3623–3634, doi:https://doi.org/10.1016/j.jmrt.2019.05.025.
55. Fodil Cherif, M.; Trache, D.; Brosse, N.; Benaliouche, F.; Tarchoun, A.F. Comparison of the Physicochemical Properties and Thermal Stability of Organosolv and Kraft Lignins from Hardwood and Softwood Biomass for Their Potential Valorization. *Waste and Biomass Valorization* **2020**, *11*, 6541–6553, doi:10.1007/s12649-020-00955-0.
56. Higgins, F.S.; Magliocco, L.G.; Colthup, N.B. Infrared and Raman Spectroscopy Study of Alkyl Hydroxamic Acid and Alkyl Hydroxamate Isomers. *Appl. Spectrosc.* **2006**, *60*, 279–287, doi:10.1366/000370206776342517.
57. Gaudin, A.M. *Flotation*; 2nd ed.; McGraw-Hill: New York, 1957;
58. Wills, B.A.; Finch, J.A. *Wills' Mineral Processing Technology: An Introduction to the Practical Aspects of Ore Treatment and Mineral Recovery*; Elsevier Inc., 2015; ISBN 9780080970530.